

PRECURSOR PLERIONIC ACTIVITY AND HIGH ENERGY GAMMA-RAY EMISSION IN THE SUPRANOVA MODEL OF GAMMA-RAY BURSTS

SUSUMU INOUE^{1,2}, DAFNE GUETTA² AND FRANCO PACINI²

submitted to Ap. J.

ABSTRACT

The supranova model of gamma-ray bursts (GRBs), in which the GRB event is preceded by a supernova (SN) explosion by a few months to years, has recently gained support from Fe line detections in X-ray afterglows. A crucial ingredient of this model yet to be studied is the fast-rotating pulsar that should be active during the time interval between the SN and the GRB, driving a powerful wind and a luminous plerionic nebula. We discuss some observational consequences of this precursor plerion, which should provide important tests for the supranova model: 1) the fragmentation of the outlying SN ejecta material by the plerion and its implications for Fe line emission; and 2) the effect of inverse Compton cooling and emission in the GRB external shock due to the plerion radiation field. The plerion-induced inverse Compton emission can dominate in the GeV-TeV energy range during the afterglow, being detectable by GLAST from redshifts $z \lesssim 1.5$ and distinguishable from self-Compton emission by its spectrum and light curve. The prospects for direct detection and identification of the precursor plerion emission are also briefly considered.

Subject headings: gamma rays: bursts, pulsars: general, stars: neutron, supernova remnants, radiation mechanisms: non-thermal, line: formation

1. INTRODUCTION

In the currently standard interpretation of gamma-ray bursts (GRBs), the central engine gives rise to a highly relativistic outflow, the ‘fireball’. Although the presence of relativistic outflows in GRBs has been amply demonstrated by multiwavelength observations of afterglows (Piran 1999, van Paradijs, Kouveliotou & Wijers 2000, Meszaros 2001), the nature of the central engine itself is still a great mystery. One model of the central engine that has recently gained attention is the ‘supranova’ model of Vietri & Stella (1998, hereafter VS98), in which a massive star ends up in a supernova (SN), but the subsequent black hole formation and GRB event is delayed by some time t_p , typically expected to be a few months to years. The SN is assumed to leave behind a rotationally-supported, ‘supramassive’ neutron star (SMNS; hereafter also referred to simply as ‘pulsar’) which then slowly shrinks by shedding angular momentum via a magnetospheric wind. (See comments on the possibility of angular momentum loss through gravitational radiation in Sec.5.) After a spin-down time t_p when roughly half its initial angular momentum has been lost, the configuration becomes unstable and collapses to a black hole with a surrounding disk, leading to the GRB proper. The model’s major advantage lies in the potential realization of a very baryon-clean pre-GRB environment (mandatory for generating sufficiently relativistic fireballs): first the SN ejects the majority of the outlying mass of the progenitor star, and second the SMNS driven-wind effectively sweeps up remaining baryonic matter in the vicinity of the central object. Support for this model comes from recent detections of strong Fe emission features in the X-ray af-

terglow spectra of some GRBs (Piro et al. 1999, Antonelli et al. 2001, Yoshida et al. 2001), particularly that of GRB991216 (Piro et al. 2000), as well as a transient Fe absorption feature in the prompt emission of GRB990705 (Amati et al. 2000), indicating surprisingly large amounts of Fe-rich material existing nearby, yet relatively removed from the GRB site. Observational constraints on its location, quantity, density and velocity are compatible with the pre-ejected shell SN remnant (SNR) in the supranova model (Lazzati et al. 1999, Vietri et al. 2001, Lazzati et al. 2001), but may be difficult to accomodate in other models (see however Rees & Mészáros 2000, Mészáros & Rees 2001, Böttcher & Fryer 2001).

The precursor pulsar wind should be extremely powerful. Before collapsing, the SMNS must inevitably expel a substantial fraction of its rotational energy E_p as a magnetically-driven wind,

$$E_p = \frac{GjM^2\omega}{2c} \sim 2.4 \times 10^{53} \text{erg } j_{0.6} M_3^2 \omega_4, \quad (1)$$

where $M = 3M_3M_\odot$ and $\omega = 10^4\omega_4\text{s}^{-1}$ are the SMNS’s mass and angular velocity, $j = 0.6j_{0.6}$ is its angular momentum in units of GM^2/c , and the numbers are typical SMNS model values (Salgado et al. 1994, Cook, Shapiro & Teukolsky, VS98). The spin-down time (i.e. the SN-GRB delay time) and corresponding wind luminosity can be estimated from the magnetic dipole formula (Pacini 1967, VS98)

$$t_p = \frac{3Gc^2jM^2}{B_*^2R_*^6\omega^3} \sim 40\text{days } j_{0.6} M_3^2 R_{*,15}^{-6} \omega_4^{-3} B_{*,13}^{-2}, \quad (2)$$

¹Division of Theoretical Astrophysics, National Astronomical Observatory, 2-21-1 Ohsawa, Mitaka, Tokyo, Japan 181-8588; inoue@th.nao.ac.jp

²Osservatorio Astrofisico di Arcetri, Largo E. Fermi, 5. 50125 Firenze, Italy; dafne@arcetri.astro.it; pacini@arcetri.astro.it; salvati@arcetri.astro.it

and

$$L_p = E_p/t_p = \frac{B_*^2 R_*^6 \omega^4}{6c^3} \sim 7.1 \times 10^{46} \text{ergs}^{-1} R_{*,15}^6 \omega_4^4 B_{*,13}^2, \quad (3)$$

where $R_* = 15R_{*,15}\text{km}$ is a typical SMNS equatorial radius. The surface magnetic field $B_* = 10^{13}B_{*,13}\text{G}$ is unconstrained from model calculations and can be considered a free parameter. Equivalently, we may take t_p as the free parameter, and vary $L_p = E_p/t_p$ accordingly with E_p fixed as in eq.1; the fiducial value we choose below is $t_p \sim 120\text{days}$ (implying $L_p \sim 2.3 \times 10^{46}\text{erg s}^{-1}$) so as to be consistent with observations of GRB991216 (see Sec.3.2). During t_p , L_p is expected to be relatively constant, and the wind should energize a plerionic nebula in the pre-GRB surroundings, a more compact yet much more luminous version of the Crab nebula.

The consequences of such a precursor plerion in the supranova scenario has not been considered previously, and this paper addresses some important dynamical and radiative effects it may induce, each providing important observational diagnostics for the supranova model. We discuss the acceleration and fragmentation of the SN ejecta material by the plerion-SNR interaction and its implications for Fe line emission in Sec.2, and inverse Compton scattering of the ambient plerion radiation field in the GRB external shock and the resulting high-energy afterglow emission in Sec.3. A brief consideration of the direct detection and identification of the precursor plerion emission is given in Sec.4. We will assume a lambda cosmology with $\Omega = 0.3$, $\Lambda = 0.7$ and $H_0 = 70\text{kms}^{-1}\text{Mpc}^{-1}$.

2. DYNAMICAL EFFECTS OF THE PLERION ON THE SUPERNOVA REMNANT

An exemplary case of the dynamical interaction between a plerion and a SNR can be seen in the well-studied Crab nebula, which is known to be accelerating and fragmenting the surrounding SNR, resulting in the prominent optical filaments instead of a clear shell (e.g. Davidson & Fesen 1985, Hester et al. 1996). In this respect, the powerful supranova plerion should be even more effective than the Crab. We model the plerion in a simple way following Pacini & Salvati (1973, hereafter PS73; see also Bandiera, Pacini & Salvati 1984, Chevalier & Reynolds 1984, Amato et al. 2000), considering a homogeneous, spherical bubble into which energy is injected at a constant rate $L_p = 10^{46}L_{p,46}\text{ergs}^{-1}$, a fraction $\xi_B = 0.5\xi_{B,0.5}$ going into magnetic field and the rest $\xi_e = 1 - \xi_B = 0.5\xi_{e,0.5}$ into relativistic electrons. The electrons here are mostly radiative (see Sec.3), so their pressure can be neglected. As the plerionic bubble initially plows through the expanding core and envelope of the progenitor star, it should accelerate the swept-up ejecta material (Chevalier 1977, Chevalier & Fransson 1992), perhaps to velocities consistent with $v_s \sim 0.05 - 0.1c$ inferred from the observed width of the Fe line in GRB991216 (Piro et al. 2000). As in the Crab, the SN ejecta will not remain as a spherical shell during this acceleration phase due to Rayleigh-Taylor (RT) instabilities operating at the plerion-SNR interface. The growth timescale of the RT instability on a spatial scale R is $t_{RT} \sim (R/\ddot{R})^{1/2}$, and since $\ddot{R} \sim 4\pi R^2 p_p/M_s$, $p_p = B_p^2/8\pi$ being the plerion magnetic pressure, its ratio

to the expansion timescale $t_{exp} \sim R/v_s$ is

$$\begin{aligned} \frac{t_{RT}}{t_{exp}} &\sim \left(\frac{2M_s v_s^2}{B_p^2 R^3} \right)^{1/2} \sim \left(\frac{2E_s}{3\xi_B E_p} \right)^{1/2} \\ &\sim 0.28 E_{s,51}^{1/2} (\xi_{B,0.5} L_{p,46})^{-1/2} t_{10}^{-1/2} \end{aligned} \quad (4)$$

(Bandiera, Pacini & Salvati 1983), where M_s , v_s and $E_s = M_s v_s^2/2 \sim 10^{51}E_{s,51}\text{erg}$ are the SNR ejecta mass, velocity and kinetic energy, and t_{10} is time after the SN measured in 10 days. In the case of the Crab, $t_{RT}/t_{exp} \gtrsim 1$ and the RT instability is just setting in, consistent with other lines of evidence (Hester et al. 1996, Sankrit & Hester 1997). However, it should develop much more rapidly for the supranova plerion. The final outcome of the instability will depend on its non-linear behavior as well as other processes such as cooling, but judging from the Crab's optical filaments, it is highly probable that the plerion will effectively shred the SNR into condensed fragments and completely engulf them during its lifetime t_p .

This has important implications for the Fe line emission in afterglows. The simplest explanation for the lines is Fe K α multiple recombination radiation from Fe-rich matter photoionized by the X-ray afterglow continuum on timescales of days (Lazzati et al. 1999, Weth et al. 2000, Paerels et al. 2000). Consistency with observations require that the material to be illuminated is very dense and possesses a large covering factor, and yet that the GRB line of sight is devoid of any such matter so that the GRB blastwave will not be decelerated too quickly (Lazzati et al. 1999). The filamentary fragmentation of the SNR may naturally account for such a geometry.

The condensation of the SNR matter may also enhance the line emissivity. The emission rate of line photons through recombination when a sufficient photoionizing flux irradiates material with electron density $n_e = 10^9 n_{e,9}\text{cm}^{-3}$ and temperature $T = 10^7 T_7 K$ containing an Fe mass $M_{\text{Fe}} = 0.1 M_{\text{Fe},0.1} M_\odot$ is

$$\dot{N}_{\text{line}} = N_{\text{Fe}}/t_{\text{rec}} \sim 1.5 \times 10^{52} \text{s}^{-1} M_{\text{Fe},0.1} n_{e,9} T_7^{-3/4} \quad (5)$$

where N_{Fe} is the total number of Fe atoms and $t_{\text{rec}} \sim 127\text{s } T_7^{3/4} n_{e,9}^{-1}$ is the recombination time (Paerels et al. 2000, Vietri et al. 2001). By the time of the GRB at $t_p \sim 120t_{p,120}\text{days}$ (see Sec.3), a SNR of $M_s \sim 10M_{s,10}M_\odot$ expanding at $v_s = 0.1v_{s,0.1}c$ will have reached a radius $R_s \sim 3.1 \times 10^{16} v_{s,0.1} t_{p,120}\text{cm}$, and if distributed in a spherical shell of width $\Delta R_s \sim 0.1R_s$, its electron density would be

$$n_{e,s} \sim 5.3 \times 10^8 M_{s,10} (v_{s,0.1} t_{p,120})^{-3} \text{cm}^{-3}. \quad (6)$$

Typically observed line fluxes can be obtained for $M_{\text{Fe},0.1} \gtrsim 4$ (Eq.5), but only if the entire spherical shell is irradiated and emits line photons efficiently. The GRB blast wave must then be isotropic and no beaming is allowed (Piro et al. 2000), which is incongruous with recent evidence to the contrary (e.g. Panaitescu & Kumar 2001, Frail et al. 2001). However, if the SNR ejecta can be condensed into filaments of much higher density, t_{rec} is shortened, and irradiating a smaller fraction of material may suffice to produce the observed lines. For comparison, the density of the Crab's optical filaments averaged over the volume of the whole nebula is $n \sim 10\text{cm}^{-3}$,

whereas the actual density of the individual filaments is $n \sim 10^3 \text{cm}^{-3}$ (Davidson & Fesen 1985). Although detailed modeling is necessary for quantitative predictions, we may speculate that the density contrast could be even higher for the supranova plerion due to the instability being more developed, and beaming fractions of order ~ 0.01 could be entirely compatible with the observed Fe lines. Note that in explaining the transient Fe absorption feature in GRB990705, Lazzati et al. (2001) have inferred the presence of clumpy SNR ejecta material with density contrasts of order 100-1000 surrounding the burst site. We also mention that even when circumstances conducive to Fe line emission cannot be realized, the action of the plerion for $t_p \gtrsim 10^3 \text{s}$ can expel much of the baryons surrounding the GRB site out to radii $\gtrsim 10^{13} \text{cm}$ and clear the path for the ensuing fireball, which is a great advantage of the supranova model.

3. EXTERNAL COMPTON COOLING AND EMISSION DUE TO THE PLERION RADIATION FIELD

Another important implication of the precursor plerion in the supranova model is that the GRB should be exploding into a ‘radiation-rich’ environment, i.e. into the luminous radiation field of the plerion, which can constitute a large fraction of the pulsar wind luminosity. Such ‘external’ photons impinging into the relativistically expanding GRB shock from outside would be seen highly Doppler-boosted in the shock comoving frame, and act as efficient seeds for inverse Compton scattering (referred to as external Comptonization, or EC), with important observational consequences for the afterglow emission. (EC processes have been extensively discussed in relation to blazars; see e.g. Sikora 1997. For previous work on EC processes in GRB shocks, see e.g. Böttcher & Dermer 1999.)

3.1. Plerion Emission

We continue the discussion of the plerion as a homogeneous, spherical bubble with constant energy injection, and estimate its radius R_p and expansion velocity v_p (or bulk Lorentz factor Γ_p) at age t_p . The plerion first penetrates through the expanding SN ejecta, effectively shredding and entraining the ejecta material within a relatively short time (eq.4). Thereafter, we may assume that it expands into the ambient interstellar medium (ISM), here taken to be uniform, and enters a deceleration stage. Since the pulsar wind is expected to be initially highly relativistic, we employ the relativistic, self-similar blastwave solution of Blandford & McKee (1976) in the case of steady, adiabatic energy injection,

$$\Gamma_p \sim (kL_p/\rho_I c^5)^{1/4} t_p^{-1/2} \sim 2.9 L_{p,46}^{1/4} n_{1,0}^{-1/4} t_{p,120}^{-1/2}, \quad (7)$$

where $n_1 = \rho_I/m_p c^2 = n_{1,0} \text{cm}^{-3}$ is the ISM density and k is a numerical factor of order unity given in Blandford & McKee (1976). This strictly applies only in the ultrarelativistic limit ($\Gamma_p \gg 1$, $v_p \sim c$); in the nonrelativistic limit ($\Gamma_p \sim 1$, $v_p \ll c$), the deceleration goes as $v_p \propto t_p^{-2/5}$ and $R_p \propto t_p^{3/5}$. In any case, for the values of L_p and n_1 considered here, the expansion of the plerionic bubble should be mildly relativistic when $t_p \sim 10^2 - 10^3 \text{days}$, so we take $v_p \sim c$ and $R_p \sim ct_p \sim 3.1 \times 10^{17} t_{p,120} \text{cm}$. (Note that the

dense, entrained SNR filaments may be moving at much lower velocities; Sec.2)

The luminosity and spectrum emitted by the plerion may be evaluated following PS73. The magnetic field inside the plerion is $B_p = (3\xi_B E_p/R_p^3)^{1/2} \sim 3.5 G \xi_{B,0.5}^{1/2} t_{p,120}^{-3/2}$, with the value of E_p fixed as in eq.1. Relativistic electrons/positrons (hereafter simply ‘electrons’) are injected into the plerion at a rate $\xi_e L_p$ with a power-law distribution $dn/d\gamma^p \propto (\gamma^p)^{-s}$ in the Lorentz factor range $\gamma_m^p \leq \gamma^p \leq \gamma_M^p$. We fiducially take $\xi_B = \xi_e = 0.5$, $s = 2$ and $\gamma_m^p = 1$, parameters which lead to consistent fits when similar models are applied to the multi-wavelength spectra of the Crab and other known plerionic nebulae (PS73, Bandiera et al. 1984, Amato et al. 2000). The maximum Lorentz factor γ_M^p is set by equating the synchrotron cooling time $t_{sy}^p \sim 6\pi m_e c/\sigma_T B_p^2 \gamma_p$ with the acceleration time, here assumed to be $t_{acc}^p \sim 2\pi \gamma_p m_e c/e B_p$ (consistent with Fermi acceleration at relativistic shocks), so that $\gamma_M^p \sim (3e/\sigma_T B_p)^{1/2}$ and the corresponding maximum synchrotron emission frequency $\nu_M^p \sim 3e^2/\pi m_e c \sigma_T \sim 1.2 \times 10^{22} \text{Hz}$. (With our fiducial choice of $\xi_B = \xi_e = 0.5$, synchrotron-self-Compton cooling is at most comparable to synchrotron cooling, so this is neglected for simplicity.) The distribution should develop a break at the Lorentz factor γ_c^p where t_{sy}^p equals the adiabatic expansion time $t_{ad}^p \sim R_p/v_p \sim t_p$. Our fiducial parameters formally result in $\gamma_c^p < 1$, implying that injected electrons of all energies are radiative and cool within t_{ad}^p , and the emission spectrum has a cooled energy index $\alpha_p \sim s/2 = 1$. The specific flux at the surface of the plerion is

$$f_{\nu^p}^p \sim \frac{\xi_e L_p (\nu^p)^{-1}}{8\pi R_p^2 \ln(\gamma_M^p/\gamma_m^p)}. \quad (8)$$

Synchrotron self-absorption will cause an effective minimum cutoff in the spectrum at a frequency

$$\nu_a^p \sim 2.4 \times 10^{11} \text{Hz} \xi_{e,0.5}^{2/7} \xi_{B,0.5}^{1/14} t_{p,120}^{-15/14}, \quad (9)$$

below which the flux falls steeply. Thus the overall plerion spectrum is that of eq.8 between ν_a^p and ν_M^p , with constant luminosity per logarithmic frequency interval, and the total emitted luminosity is of order $\xi_e L_p$. (Any flux above ν_M^p which may arise from self-Compton emission is irrelevant for electrons in the GRB shock due to Klein-Nishina effects; see below.) Note that many quantities regarding the plerion contain subscripts or superscripts p in order to avoid confusion with those for the GRB blastwave.

3.2. GRB Afterglow Emission

At time t_p after the SN, the pulsar collapses and the GRB goes off, sending a fireball and relativistic blastwave into the plerion. The deceleration of the GRB blastwave, and hence the afterglow, initiates when it has swept up enough outlying baryonic material. This may occur inside the plerion, if the (probably collimated) fireball in our line of sight happens to strike the denser parts of the entrained SN ejecta fragments, which should be clumpy and inhomogeneous (Sec.2). Alternatively, the fireball may travel unimpeded through regions of low

baryon density in the plerion, and decelerate only after making its way out into the surrounding ISM. In either case, we will assume for simplicity that the decelerating medium is uniform, at least within the timescales we consider. The standard expressions for the radius r and bulk Lorentz factor Γ of the shocked material in an adiabatic, spherical blastwave decelerating self-similarly in a uniform medium are $r(t) = [12Ect/4\pi nm_p c^2(1+z)]^{1/4} \sim 3.6 \times 10^{17} \text{cm} (E_{52}/n)^{1/4} [t_d/(1+z)]^{1/4}$ and $\Gamma(t) = [3E(1+z)^3/256\pi nm_p c^5 t^3]^{1/8} \sim 5.9 (E_{52}/n)^{1/8} [t_d/(1+z)]^{-3/8}$, respectively (e.g. Mészáros & Rees 1997, Piran 1999). Here $E = 10^{52} E_{52} \text{erg}$ is the blastwave energy, $n \text{cm}^{-3}$ the external medium density, $t = t_d \text{day}$ the observer time elapsed after the GRB, z is the GRB redshift, and we have adopted the kinematic relation $t = r(1+z)/4\Gamma^2 c$. The deceleration starts at radius $r_{dec} = (3E/4\pi nm_p c^2 \Gamma_0^2)^{1/3} \sim 2.6 \times 10^{16} \text{cm} (E_{52}/n)^{1/3} \Gamma_{0,300}^{-2/3}$ at observer time $t_{dec} = r_{dec}(1+z)/4\Gamma_0^2 c \sim 2.4 \text{s} (1+z) (E_{52}/n)^{1/3} \Gamma_{0,300}^{-8/3}$, where $\Gamma_0 = 300 \Gamma_{0,300}$ is the initial bulk Lorentz factor.

To describe the time-dependent, multiwavelength afterglow spectrum from the blastwave, we follow standard discussions of the synchrotron emission (e.g. Mészáros & Rees 1997, Sari, Piran & Narayan 1998, Wijers & Galama 1999), and extend it to include cooling and emission by the EC process in addition to the synchrotron-self-Compton (SSC) process (Panaitescu & Kumar 2000; Sari & Esin 2001, hereafter SE01; Zhang & Mészáros 2001, hereafter ZM01). It is assumed that constant fractions $\epsilon_B = 0.01 \epsilon_{B,-2}$ and $\epsilon_e = 0.1 \epsilon_{e,-1}$ of the postshock energy are imparted to magnetic field and relativistic electrons, respectively. The comoving magnetic field is $B(t) = (32\pi \epsilon_B n m_p)^{1/2} \Gamma c \sim 0.23 G \epsilon_{B,-2}^{1/2} E_{52}^{1/8} n^{3/8} [t_d/(1+z)]^{-3/8}$. Electrons are accelerated in the shock to a power-law distribution $dn/d\gamma \propto \gamma^{-p}$ in the Lorentz factor range $\gamma_m \leq \gamma \leq \gamma_M$. We assume $p > 2$, our standard choice being $p = 2.5$. The minimum Lorentz factor γ_m is given by

$$\begin{aligned} \gamma_m(t) &= \epsilon_e \Gamma(t) (m_p/m_e) (p-2)/(p-1) \\ &\sim 360 \epsilon_{e,-1} [3(p-2)/(p-1)] \\ &\quad \times (E_{52}/n)^{1/8} [t_d/(1+z)]^{-3/8} \end{aligned} \quad (10)$$

(note that $[3(p-2)/(p-1)] = 1$ when $p = 2.5$). The electrons radiatively cool by the combination of the synchrotron, SSC and EC processes, the timescales of which are $t'_{sy} \sim 6\pi m_e c / \sigma_T B^2 \gamma$, $t'_{ssc} \equiv Y t'_{sy}$ and $t'_{ec} \equiv X t'_{sy}$ respectively, the total cooling time being $t'_c = [(1/t'_{sy}) + (1/t'_{ssc}) + (1/t'_{ec})]^{-1} = t'_{sy} (1+Y+X)^{-1}$. The maximum Lorentz factor γ_M is determined by balancing t'_c with the acceleration time $t'_{acc} \sim 2\pi \gamma m_e c / eB$,

$$\begin{aligned} \gamma_M(t) &= [3e/\sigma_T B(1+Y+X)]^{1/2} \\ &\sim 0.97 \times 10^8 (1+Y+X)^{-1/2} \epsilon_{B,-2}^{-1/4} \\ &\quad \times E_{52}^{-1/16} n^{-3/16} [t_d/(1+z)]^{3/16} \end{aligned} \quad (11)$$

(ZM01). The cooling Lorentz factor γ_c is where t'_c equals the comoving adiabatic expansion time $t'_{ad} \sim r/c\Gamma \sim t\Gamma$,

$$\begin{aligned} \gamma_c(t) &= (1+Y+X)^{-1} 6\pi m_e c / \sigma_T \Gamma B^2 t \\ &\sim 2.9 \times 10^4 (1+Y+X)^{-1} \epsilon_{B,-2}^{-1} \end{aligned}$$

$$\times E_{52}^{-3/8} n^{-5/8} [t_d/(1+z)]^{1/8}. \quad (12)$$

The observed characteristic synchrotron emission frequency for an electron of Lorentz factor γ is $\nu = (4/3)\Gamma(3/4\pi)(eB/m_e c)\gamma^2(1+z)^{-1}$ (Wijers & Galama 1999), so those for each of γ_m , γ_M and γ_c are respectively

$$\begin{aligned} \nu_m(t) &\sim 1.0 \times 10^{12} \text{Hz} \epsilon_{B,-2}^{1/2} \epsilon_{e,-1}^2 [3(p-2)/(p-1)]^2 \\ &\quad \times E_{52}^{1/2} t_d^{-3/2} (1+z)^{1/2}, \end{aligned} \quad (13)$$

$$\begin{aligned} \nu_M(t) &\sim 0.72 \times 10^{23} \text{Hz} (1+Y+X)^{-1} \\ &\quad \times E_{52}^{1/8} n^{-1/8} t_d^{-3/8} (1+z)^{-5/8}, \end{aligned} \quad (14)$$

and

$$\begin{aligned} \nu_c(t) &\sim 6.4 \times 10^{15} \text{Hz} (1+Y+X)^{-2} \epsilon_{B,-2}^{-3/2} \\ &\quad \times E_{52}^{-1/2} n^{-1} t_d^{-1/2} (1+z)^{-1/2}. \end{aligned} \quad (15)$$

At early times ($t < t_t$), $\gamma_m > \gamma_c$, and all electrons cool within t'_{ad} (fast cooling regime). The synchrotron flux f_ν then peaks at ν_c and mainly consists of three power-law segments: $f_\nu = (\nu/\nu_c)^{1/3} f_{\nu,\max}$ for $\nu < \nu_c$, $f_\nu = (\nu/\nu_c)^{-1/2} f_{\nu,\max}$ for $\nu_c < \nu < \nu_m$ and $f_\nu = (\nu_m/\nu_c)^{-1/2} (\nu/\nu_m)^{-p/2} f_{\nu,\max}$ for $\nu_m < \nu < \nu_M$. At late times ($t > t_t$), $\gamma_m < \gamma_c$, and only electrons of $\gamma > \gamma_c$ cool within t'_{ad} (slow cooling regime). Then the spectrum peaks at ν_m , and again has three parts: $f_\nu = (\nu/\nu_m)^{1/3} f_{\nu,\max}$ for $\nu < \nu_m$, $f_\nu = (\nu/\nu_m)^{-(p-1)/2} f_{\nu,\max}$ for $\nu_m < \nu < \nu_c$ and $f_\nu = (\nu_c/\nu_m)^{-(p-1)/2} (\nu/\nu_c)^{-p/2} f_{\nu,\max}$ for $\nu_c < \nu < \nu_M$. The peak synchrotron flux $f_{\nu,\max}$ for either fast or slow cooling is

$$\begin{aligned} f_{\nu,\max} &= CTBr^3(1+z)/D^2 \\ &\sim 2.9 \text{mJy} \epsilon_{B,-2}^{1/2} E_{52} n^{1/2} D_{28}^{-2} (1+z), \end{aligned} \quad (16)$$

where C is a numerical constant and $D = 10^{28} D_{28} \text{cm}$ is the distance to the GRB. The transition from fast to slow cooling ($\gamma_c = \gamma_m$) occurs at the time

$$\begin{aligned} t_t &\sim 13 \text{s} (1+Y+X)^2 \epsilon_{B,-2}^2 \epsilon_{e,-1}^2 [3(p-2)/(p-1)]^2 \\ &\quad \times E_{52} n (1+z). \end{aligned} \quad (17)$$

(Synchrotron self-absorption should cause an additional spectral break at the lowest frequencies, but is ignored here as it is observationally irrelevant for the high energy afterglow emission, our main concern.)

To account for the effects of EC and SSC cooling, we have introduced X and Y , which are in general time-dependent. The EC parameter X equals the ratio of comoving frame energy density in plerion radiation field u'_p to that in magnetic field u'_B . If the blastwave decelerates inside the plerion ($r < R_p$), which is the case mainly considered below, we may presume that the radiation field is nearly uniform and isotropic, obtaining

$$\begin{aligned} X &\sim \frac{u'_p}{u'_B} \sim \Gamma^2 \frac{\xi_e L_p}{4\pi R_p^2 c} \\ &\quad \times \frac{\ln(\min\{\nu'_M, \nu'_{KN}\}/\nu'_a)}{2 \ln(\gamma'_M/\gamma'_m)} / 4\epsilon_B \Gamma^2 n m_p c^2, \end{aligned} \quad (18)$$

where $\nu_{KN}^p \sim m_e c^2 / h\gamma$ is the frequency above which Klein-Nishina (KN) effects suppress Compton scattering, depending on γ . Observe here that the factors of Γ^2 in u'_p and u'_B cancel out so that aside from the weak t -dependence through ν_{KN}^p , X is constant in time. Generally $\nu_M^p > \nu_{KN}^p$, but we do not make large errors in taking $\min\{\nu_M^p, \nu_{KN}^p\} \sim \nu_M^p$ in the logarithmic factor for simplicity. For a blastwave decelerating outside the plerion ($r > R_p$), the radiation field is anisotropic and falls with r , and X differs from eq.18 by a factor of $\sim (R_p/r)^2(1 - 2\mu + 4\mu^2)/3$ where $\mu = \sqrt{1 - (R_p/r)^2}$ (which applies for $\Gamma \gg 1$; see e.g. Sikora et al. 1996, Inoue & Takahara 1997), decreasing with time.

The SSC parameter Y can be evaluated as in SE01, $Y \sim u'_{sy}/u'_B \sim \eta u'_e/[u'_B(1+Y+X)] \sim \eta \epsilon_e/[\epsilon_B(1+Y+X)]$, where u'_e and u'_{sy} are the comoving frame energy densities in relativistic electrons and synchrotron radiation, and $\eta \sim \min\{1, (\gamma_c/\gamma_m)^{2-p}\}$ is the fractional energy radiated by electrons. In the fast cooling phase, $\eta \sim 1$ and we get the expression

$$Y \sim \frac{1}{2} \left(\sqrt{4\epsilon_e/\epsilon_B + (1+X)^2} - 1 - X \right). \quad (19)$$

In the slow cooling phase, Y decreases with time but only very slowly for typical values of p (SE01), so we simplify by assuming eq.19 at all times.

The SSC spectrum has a similar shape to the synchrotron spectrum, and we approximate it as comprising broken power-laws (SE01, ZM01), with characteristic frequencies at

$$\begin{aligned} \nu_m^{SC} &\sim \gamma_m^2 \nu_m \\ &\sim 1.2 \times 10^{17} \text{Hz} \epsilon_{e,-1}^4 \epsilon_{B,-2}^{1/2} [3(p-2)/(p-1)]^4 \\ &\times E_{52}^{3/4} n^{-1/4} t_d^{-9/4} (1+z)^{5/4} \end{aligned} \quad (20)$$

and

$$\begin{aligned} \nu_c^{SC} &\sim \gamma_c^2 \nu_c \\ &\sim 5.4 \times 10^{24} \text{Hz} (1+Y+X)^{-4} \epsilon_{B,-2}^{-7/2} \\ &\times E_{52}^{-5/4} n^{-9/4} t_d^{-1/4} (1+z)^{-3/4}. \end{aligned} \quad (21)$$

The maximum SSC frequency should occur at

$$\begin{aligned} \nu_{KN} &\sim \Gamma \gamma_M m_e c^2 (1+z)^{-1} \\ &\sim 0.71 \times 10^{28} \text{Hz} (1+Y+X)^{-1/2} \epsilon_{B,-2}^{-1/4} \\ &\times E_{52}^{1/16} n^{-5/16} t_d^{-3/16} (1+z)^{-13/16}, \end{aligned} \quad (22)$$

where KN effects completely cut off the spectrum. (Generally, $\nu_{KN} \ll \nu_M^{SC} \sim \gamma_M^2 \nu_M$.) For fast cooling, the SSC flux f_ν^{SC} peaks at ν_c^{SC} , the spectrum being $\propto \nu^{1/3}$ for $\nu < \nu_c^{SC}$, $\propto \nu^{-1/2}$ for $\nu_c^{SC} < \nu < \nu_m^{SC}$ and $\propto \nu^{-p/2}$ for $\nu_m^{SC} < \nu < \nu_{KN}$; for slow cooling, the peak is at ν_m^{SC} , and the spectrum is $\propto \nu^{1/3}$ for $\nu < \nu_m^{SC}$, $\propto \nu^{-(p-1)/2}$ for $\nu_m^{SC} < \nu < \nu_c^{SC}$ and $\propto \nu^{-p/2}$ for $\nu_c^{SC} < \nu < \nu_{KN}$. The peak SSC flux $f_{\nu,\max}^{SC}$ is equal to the peak synchrotron $f_{\nu,\max}$ multiplied by the optical depth τ_e of the shocked material,

$$\begin{aligned} f_{\nu,\max}^{SC} &\sim \tau_e f_{\nu,\max} \sim (\sigma_T n r / 3) f_{\nu,\max} \\ &\sim 2.3 \times 10^{-9} \text{mJy} \epsilon_{B,-2}^{1/2} E_{52}^{5/4} n^{5/4} D_{28}^2 t_d^{1/4} (1+z)^{3/2} \end{aligned}$$

The EC spectrum reflects the shapes of both the electron distribution and the plerion spectrum. Considering deceleration inside the plerion, and again adopting the broken power-law approximation, spectral breaks arise at the frequencies where electrons of γ_m and γ_c upscatter plerion photons of ν_a^p ,

$$\begin{aligned} \nu_m^{EC} &\sim \gamma_m^2 \Gamma^2 \nu_a^p (1+z)^{-1} \\ &\sim 1.1 \times 10^{18} \text{Hz} \epsilon_{e,-1}^2 [3(p-2)/(p-1)]^2 \\ &\times E_{52}^{1/2} n^{-1/2} t_d^{-3/2} (1+z)^{1/2} \end{aligned} \quad (24)$$

and

$$\begin{aligned} \nu_c^{EC} &\sim \gamma_c^2 \Gamma^2 \nu_a^p (1+z)^{-1} \\ &\sim 0.71 \times 10^{22} \text{Hz} (1+Y+X)^{-2} \epsilon_{B,-2}^{-2} \\ &\times E_{52}^{-1/2} n^{-3/2} t_d^{-1/2} (1+z)^{-1/2}, \end{aligned} \quad (25)$$

where the fiducial numerical value for ν_a^p in eq.9 has been used. Note the factor Γ^2 which results from two Lorentz transformations, one into the comoving frame from the observer frame and another vice-versa. The fast cooling EC spectrum has a peak flux at ν_c^{EC} , is $\propto \nu$ for $\nu < \nu_c^{EC}$ from the behavior of the Compton scattering cross section, $\propto \nu^{-1/2}$ for $\nu_c^{EC} < \nu < \nu_m^{EC}$ and $\propto \nu^{-1}$ for $\nu_m^{EC} < \nu < \nu_{KN}$, mirroring the flat plerion spectrum. The KN limit discussed above also applies here for the maximum EC frequency, ν_M^p being irrelevant. Likewise, the slow cooling EC spectrum peaks at ν_m^{EC} , and is $\propto \nu$ for $\nu < \nu_m^{EC}$, $\propto \nu^{-(p-1)/2}$ for $\nu_m^{EC} < \nu < \nu_c^{EC}$ and $\propto \nu^{-1}$ for $\nu_c^{EC} < \nu < \nu_{KN}$. The peak EC flux $f_{\nu,\max}^{EC}$ may be obtained analogously to the SSC case, but using the relation $f_{\nu',\max}^{EC} \sim \tau_e f_{\nu',\max}^p$ in the comoving frame, where $f_{\nu',\max}^p \sim \Gamma f_{\nu,\max}^p$ is the the peak plerion flux emitted at $\nu'^p = \nu_a^p \sim \Gamma \nu_a^p$. Accounting for Lorentz transformations to and from the comoving frame,

$$f_{\nu,\max}^{EC} \sim \Gamma^2 \tau_e f_{\nu,\max}^p \frac{r^2}{D^2} (1+z) \quad (26)$$

$$\begin{aligned} &= \Gamma^2 \frac{\sigma_T n r}{3} \frac{\xi_e L_p (\nu_a^p)^{-1}}{8\pi R_p^2 \ln(\gamma_M^p/\gamma_m^p)} \frac{r^2}{D^2} (1+z) \\ &\sim 2.3 \times 10^{-3} \text{mJy} E_{52} D_{28}^2 (1+z), \end{aligned} \quad (27)$$

where the last line assumes fiducial plerion parameters. (Being isotropic in the observer frame, the plerion radiation field should be highly anisotropic in the shock frame moving at $\Gamma \gg 1$. Instead of an accurate but cumbersome calculation of the Compton upscattered photon distribution including the full angle-dependence, we have approximated by using quantities averaged over angles in the comoving frame; see e.g. Dermer 1995, Inoue & Takahara 1996, Sikora 1997.)

The broken power-law representations of the EC and SSC spectra should be adequate to within an order of magnitude, but more accurate calculations properly integrating over the broad seed photon frequency distribution will result in smoother spectral breaks and somewhat larger fluxes (above ν_c^{EC} and ν_c^{SC} for fast cooling, or above

ν_m^{EC} and ν_m^{SC} for slow cooling) due to logarithmic terms contributed by a range of electron Lorentz factors (SE01). Regarding KN effects, a gradual steepening from $\nu \lesssim \nu_{KN}$ instead of an abrupt cutoff should actually occur, as parts of the seed photon spectra will be in the KN regime even for electrons with $\gamma \lesssim \gamma_M$. We have not included the effects of internal pair attenuation, which could be important for the highest emission energies at relatively early times in the afterglow. However, significant differences are expected only for TeV energies and above (ZM01), whereby pair degradation by the infrared background during intergalactic propagation should be serious anyway for GRBs with $z \gtrsim 0.1$ (e.g. Stecker & de Jager 1998, Totani 2000).

Having laid out the tools to calculate the broadband afterglow emission, we now discuss some constraints to be imposed on the local environment of the blastwave in the context of our model. For an afterglow to produce a strong Fe line as observed in GRB991216, it is necessary that the GRB blastwave decelerates inside the plerion near relatively dense SNR fragments, so that they are irradiated efficiently by afterglow continuum X-rays. The local baryon density in the plerion interior may range anywhere from values as high as $n \sim 10^{11} \text{cm}^{-3}$ for the densest SNR clumps, to much lower values $n \ll 1 \text{cm}^{-3}$ for regions efficiently swept out by the magnetized plerionic plasma. If the local density in our line of sight $n \gtrsim 10^6 \text{cm}^{-3}$, the blastwave turns subrelativistic in less than ~ 1 day and is unable to generate the observed afterglows (Lazzati et al. 1999; see however Masetti et al. 2001, In 't Zand et al. 2001), whereas if the density $n \lesssim 10^{-3} \text{cm}^{-3}$, the blastwave does not decelerate significantly until it reaches the ISM outside the plerion at $r > R_p$. We fiducially choose $n \sim 10^3 \text{cm}^{-3}$, so that the blastwave travels from $r \sim 3 \times 10^{15} \text{cm}$ to $\sim 6 \times 10^{16} \text{cm}$ during $t \sim 0.2$ s to ~ 2 days inside the plerion, illuminating nearby Fe-rich condensations along the way, and turns subrelativistic ($\Gamma \sim 1$) at $t \sim 15$ days. A further requirement is that t_p should be neither much shorter nor much longer than ~ 120 days: $t_{p,120} \ll 1$ would not allow time for enough SN-synthesized radioactive Co to decay to Fe (Vietri et al. 2001), whereas for $t_{p,120} \gg 1$ the SNR fragments would be of too low density to generate the observed Fe line flux, unless they can be made extremely condensed (eqs.5,6). This justifies our fiducial choice of $t_{p,120} = 1$. (These conditions may be consistent with the time-delay and ionization parameter constraints discussed e.g. in Piro et al. (2000) and Vietri et al. (2001), since they apply to the distance d_i between the continuum source and the irradiated, line-emitting matter, which can be much smaller than the radius r of the matter from the GRB site. The blastwave (i.e. the continuum source) itself should have moved out to $r \gtrsim 10^{16} - 10^{17} \text{cm}$ by $t \sim 1$ day, but Fe-rich material could be present in its immediate vicinity at $d_i \ll r$.)

3.3. Results and Discussion

Guided by the observed characteristics of afterglows such as GRB991216, our fiducial parameters were chosen to represent conditions favorable for generating strong Fe lines. However, we will not attempt model fits to the available data on individual objects, since i) realistically, additional complicating effects of jet geometry, etc. can be important and must be taken into account, and ii) full pa-

rameter searches for fitting particular observations are out of our scope (c.f. Panaitescu & Kumar 2001a,b). The result given here for the fiducial parameter set is intended to exemplify some notable features of afterglows wherein EC cooling and emission induced by the supranova plerion are important. Changing these parameters can lead to either stronger or weaker EC effects (see below).

Figs.1 and 2 show our fiducial results in terms of the time-dependent broadband afterglow spectra at different observer times t , and the afterglow light curves at selected fixed frequencies, respectively, assuming the GRB to be at $z = 1$ in the lambda cosmology (i.e. $D \sim 2 \times 10^{28} \text{cm}$).

The values of X and Y are fiducially $X \sim 1.3$ and $Y \sim 2.2$, and since they were approximated as being constant, the relative luminosities of the synchrotron, SSC and EC components stay roughly the same. However, each component is prominent in a different energy band which changes with t : at the beginning of the afterglow ($t \lesssim 1$ min), the SSC component dominates at the highest energies ($\sim \text{TeV}$) whereas the EC component does so at somewhat lower energies ($\sim \text{GeV}$); in the latter stages ($t \gtrsim 1$ hr), this is reversed. The lower energies are always dominated by the synchrotron component, although the energy of the luminosity peak progressively decreases from $\sim \text{MeV}$ down to the radio band. There are clear differences between the spectral shapes of the SSC and EC components: the SSC peaks in νf_ν at $\nu^{SC} \sim \max\{\nu_m^{SC}, \nu_c^{SC}\}$ and has a steep high energy slope above this break identical to that of the synchrotron emission (energy index $-p/2$), but the EC component is flat in νf_ν above $\nu^{EC} \sim \max\{\nu_m^{EC}, \nu_c^{EC}\}$, reflecting the harder plerion spectrum. This spectral signature is one way to observationally distinguish between SSC and EC emission, even though this distinction can be blurred if values of p happen to be close to s .

Here the fast to slow cooling transition occurs at $t_t \sim 6.3$ days, and the afterglow is still fast cooling at $t \sim 1$ day. This is longer than in standard discussions, and is partly due to the extra cooling process of EC, but primarily as a consequence of the relatively high external density adopted, $n \sim 10^3 \text{cm}^{-3}$. The light curves at fixed frequencies can be described by breaks at characteristic times t_m and t_c corresponding to the passage of the minimum and cooling frequencies for each spectral component, as well as at t_t . The synchrotron light curves are as in previous studies (Sari et al. 1998): for high frequencies in which $t_c < t_m < t_t$, $f_\nu \propto t^{1/6}$ for $t < t_c$, $f_\nu \propto t^{-1/4}$ for $t_c < t < t_m$ and $f_\nu \propto t^{(2-3p)/4} [t^{-1.38}]$ for $t > t_m$; for low frequencies in which $t_t < t_m < t_c$, $f_\nu \propto t^{1/6}$ for $t < t_t$, $f_\nu \propto t^{1/2}$ for $t_t < t < t_m$, $f_\nu \propto t^{(3-3p)/4} [t^{-1.13}]$ for $t_m < t < t_c$ and $f_\nu \propto t^{(2-3p)/4} [t^{-1.38}]$ for $t > t_c$. In these expressions and below, the t -dependence inside the brackets are for our standard choice of $s = 2$ and $p = 2.5$. Defining t_c^{SC} , t_m^{SC} as times when $\nu = \nu_c^{SC}$, ν_m^{SC} respectively, the SSC light curves are: for high frequencies in which $t_c^{SC} < t_m^{SC} < t_t$,

$$f_\nu^{SC} \propto \begin{cases} t^{1/3} & t < t_c^{SC} \\ t^{1/8} & t_c^{SC} < t < t_m^{SC} \\ t^{(10-9p)/8} [t^{-1.56}] & t > t_m^{SC}; \end{cases} \quad (28)$$

for low frequencies in which $t_t < t_m^{SC} < t_c^{SC}$,

$$f_\nu^{SC} \propto \begin{cases} t^{1/3} & t < t_t \\ t & t_t < t < t_m^{SC} \\ t^{(11-9p)/8} & [t^{-1.44}] t_m^{SC} < t < t_c^{SC} \\ t^{(10-9p)/8} & [t^{-1.56}] t > t_c^{SC}. \end{cases} \quad (29)$$

The EC light curves depend on the plerion spectral index ($-s/2$). With t_c^{EC} , t_m^{EC} as times when $\nu = \nu_c^{EC}$, ν_m^{EC} respectively: for high frequencies in which $t_c^{EC} < t_m^{EC} < t_t$,

$$f_\nu^{EC} \propto \begin{cases} t^{1/2} & t < t_c^{EC} \\ t^{-1/4} & t_c^{EC} < t < t_m^{EC} \\ t^{(2-3s)/4} & [t^{-1}] t_m^{EC} < t < t_t \\ t^{(2-2p-s)/4} & [t^{-1.2}] t > t_t; \end{cases} \quad (30)$$

for low frequencies in which $t_t < t_m^{EC} < t_c^{EC}$,

$$f_\nu^{EC} \propto \begin{cases} t^{1/2} & t < t_t \\ t^{3/2} & t_t < t < t_m^{EC} \\ t^{(3-3p)/4} & [t^{-1.13}] t_m^{EC} < t < t_c^{EC} \\ t^{(2-2p-s)/4} & [t^{-1.2}] t > t_c^{EC}. \end{cases} \quad (31)$$

Differences can be seen in the decay indices at late times between the SSC and EC components: $f_\nu^{SC} \propto t^{(10-9p)/8} [t^{-1.56}]$ both before and after t_t for SSC, compared to $f_\nu^{EC} \propto t^{(3-3p)/4} [t^{-1.13}]$ before t_t breaking to $f_\nu^{EC} \propto t^{(2-2p-s)/4} [t^{-1.2}]$ after t_t for EC. These features should be important observational diagnostics in the X-ray and gamma-ray range, although here again, the discrimination is less clear if p approaches s . (Note also that there should actually be a slight break in the SSC light curve at t_t from the time-dependence of Y ; SE01.) The generally harder spectrum of the EC emission relative to SSC should make it increasingly dominant in the higher energy bands at later times.

The early X-ray and optical emission is predominantly synchrotron, but the entry of the minimum frequency of the SSC emission (and to a lesser extent, the EC emission) gives rise to ‘bumps’ in the light curves, which appear at $t \sim 0.5$ days in X-rays and $t \sim 10$ days in the optical for our fiducial calculation. In particular, we see that X-ray emission after ~ 1 day is SSC plus EC emission. So far, there have been no clear indications for such X-ray bumps, except for a flattening in the X-ray light curve of GRB000926 at $t \sim 2$ days. Together with multiwavelength spectra, this has been interpreted as SSC emission from a blastwave in a moderately dense medium of $n \sim 30\text{cm}^{-3}$ (Harrison et al. 2001), but a different explanation with an even denser medium ($n \sim 4 \times 10^4\text{cm}^{-3}$) is also possible (Piro et al. 2001). In the optical band, it is interesting to recall that a small number of afterglows have been seen to exhibit bumps at few tens of days, attributable to an underlying supernova light curve superimposed on the afterglow (e.g. Bloom et al. 1999, Galama et al. 2000, Lazzati et al. 2001b). The observed bumps seem to manifest simultaneous spectral reddening, as opposed to the spectral hardening expected for the SSC induced bumps. However, with the exception of GRB980326, the combined evidence for light curve bump plus reddening is not very strong, so an SSC explanation may not be ruled out, at least for some of the observations. In any case, realistic

modeling of light curve breaks should also include other effects such as jet geometry, so firm conclusions in comparison with observations are not possible at the moment.

The detection of the EC component, which is distinctive to the supranova model, should be best achieved at GeV energies and above. We can assess the detectability in GeV gamma-rays by the EGRET and GLAST instruments, following the discussion of ZM01. The fluence threshold of each instrument are described by a constant value for photon-limited, short integration times and one proportional to $t^{1/2}$ for background-limited, long integration times. This can be compared with the model fluence light curves, integrated over the energy range of 400 MeV to 200 GeV. Our fiducial model would have been observable by EGRET hours after the GRB from $z \lesssim 0.5$, providing a viable explanation for the extended GeV emission seen in GRB940217 (Hurley et al. 1994). GLAST should be able to detect this from redshifts as high as $z \sim 1.5$ up to ~ 1 day after the burst.

We now discuss the effect of changing our main free parameters, particularly those regarding the plerionic environment, n and t_p . Keeping all others constant, decreasing n from $n \sim 10^3\text{cm}^{-3}$ leads to a greater dominance of the EC component and less synchrotron emission, as this implies a smaller B and larger X for the same ϵ_B . Higher values of n may also occur inside the plerion; note the recent observations of GRB010222 indicating $n \sim 10^6\text{cm}^{-3}$ for this burst (Masetti et al. 2001, In ’t Zand et al. 2001). More ‘conventional’ parameters (lower n , small X) may be accommodated in the context of our model by taking a larger t_p to make $u_p \propto L_p/R_p^2 \propto t_p^{-3}$ smaller, say $t_p \sim 3\text{yr}$, and assuming $n \sim 1\text{cm}^{-1}$. However, in this case the volume-averaged SN ejecta density should also drop (eq.6), so that strong Fe lines are less likely, requiring extreme clumping of ejecta material. Note that clear upper limits on Fe line emission obtained for some bright afterglows point to a variety of GRB environments (Yonetoku et al. 2000, 2001), which could correspond to a range of t_p and/or n in our model. We also mention that the well observed afterglow of GRB970508 has an Fe line feature detection (Piro et al. 1999), as well as arguments for consistency with more or less ‘standard’ parameters (Wijers & Galama 1999), but including the effects of SSC and EC cooling in the model fitting may allow different sets of parameters (e.g. SE01).

4. DIRECT DETECTABILITY OF THE PRECURSOR PLERION

Finally, we briefly remark on the possibility of the direct detection and identification of the precursor plerion emission, which would be a straightforward test for the supranova model (c.f. VS98). As discussed above, the plerion should be a luminous, steady source during a period t_p prior to the burst, typically with bolometric luminosity $\sim \xi_e L_p \sim 10^{46}\text{ergs}^{-1} t_{p,120}^{-1}$ and power-law spectrum of energy index ~ -1 between frequencies $\sim 10^{11}\text{Hz}$ and $\sim 10^{22}\text{Hz}$. This is comparable to high-luminosity quasars and readily observable; e.g. it should have already been detected out to $z \sim 0.7$ as bright keV X-ray sources during the ROSAT All-Sky Survey (RASS; Voges et al. 1999). The event rate of GRBs detectable by BATSE from $z \lesssim 0.7$ may be roughly $R_{GRB} \sim 30\text{yr}^{-1}$ all-sky (e.g. Porciani & Madau 2001), so there should always be at

least $R_{GRB}t_p/f_b \sim 10f_b^{-1}$ active plerions all-sky above the RASS sensitivity. Here f_b^{-1} is inverse of the fractional solid angle subtended by the GRB beam, which could be as large as ~ 100 (Frail et al. 2001), and we have assumed that the plerions are not strongly beamed (c.f. eq.7). However, the problem lies in ascertaining these sources as precursors to GRBs, which must be shown to be positionally coincident as well as correlated in time within t_p before the GRB. Even though the operation periods of BATSE and RASS were close enough in time, the large BATSE error boxes ($\Delta\theta \sim 1^\circ$) preclude discrimination from the large number of AGNs with similar X-ray spectra. More precise GRB localizations by present and next generation instruments (e.g. HETE-2 with $\Delta\theta \sim 10'' - 10'$ or Swift with $\Delta\theta \sim 1'' - 4'$), combined with concurrently conducted wide field X-ray surveys (e.g. XMM-Newton serendipitous survey) should improve the prospects on searching for GRB - precursor plerion associations.

The plerion should also be conspicuous in the optical, e.g. its R-band magnitude would be $R_c \sim 17$ at $z \sim 1$. (The precursor supernova may be observable as well, but could be masked by the luminous plerion.) Again, identifying these with the ensuing GRB out of the numerous other objects at similar magnitudes requires accurate GRB positions and nearly contemporaneous wide field optical surveys. This may be possible through serendipitous studies of observations made by e.g. the Subaru Suprime-Cam, the Sloan Digital Sky Survey, and the future Supernova Acceleration Probe mission.

5. SUMMARY AND COMMENTS

We summarize the salient points of our work. In the supranova model of GRBs, the fast-rotating SMNS active during the time between the SN and the GRB should drive a luminous plerionic nebula into the preburst environment, with a number of important consequences for the ensuing

GRB afterglow. Rayleigh-Taylor instabilities acting at the plerion-SN ejecta interface can induce significant filamentary clumping of the ejecta material, allowing a favorable geometry and enhanced emissivity for the afterglow Fe line emission. The plerion radiation field can act as seeds for EC cooling and emission in the GRB external shock, leading to prominent GeV-TeV gamma-rays during the afterglow, which is detectable by GLAST out to typical GRB redshifts, and distinguishable from SSC emission by its characteristic spectrum and light curve. A direct search for the plerion emission prior to the GRB may be conducted through accurate GRB positions and concurrent wide field surveys, e.g. in the optical and X-rays. All of these should provide critical tests for the supranova model in the near future.

Although we have concentrated on the case of the pulsar spinning down exclusively via a magnetospheric wind, there is a possibility that significant spindown can also occur through gravitational wave emission, such as those driven by r-mode instabilities (e.g. Andersson et al. 2000, Stergioulas & Font 2001, Lindblom, Tohline & Vallisneri 2001 and references therein). However, many aspects of the present theoretical calculations regarding gravitational waves are uncertain (Fryer & Woosley 2001). Our work can be viewed as exploring the maximum possible effects of electromagnetic spindown, which can be modeled with some more confidence. In reality, both effects could be important to varying degrees, and we leave an investigation of such cases to the future.

We are thankful to M. Salvati for initially suggesting the possibility of EC processes in the supranova model, and E. Amato for helpful discussions. S.I. also expresses his heartfelt thanks to members of the Arcetri Astrophysical Observatory for a very pleasant and hospitable environment where part of this work was carried out.

REFERENCES

- Amati, L. et al. 2000, *Sci.*, 290, 953
 Amato, E., Salvati, M., Bandiera, R., Pacini, F. & Woltjer, L. 2000, *A&A*, 359, 1107
 Andersson, N., Jones, D. I., Kokkotas, K. & Stergioulas, N. 2000, *ApJ*, 534, L75
 Antonelli, L. A. et al. 2001, *ApJ*, 545, L39
 Bandiera, R., Pacini, F. & Salvati, M. 1983, *A&A*, 126, 7
 Bandiera, R., Pacini, F. & Salvati, M. 1984, *ApJ*, 285, 134
 Björnsson, C.-I. 2001, *ApJ*, 554, 593
 Blandford, R. D. & McKee, C. F. 1976, *Phys. Fluids*, 19, 1130
 Bloom, J. S. et al. 1999, *Nature*, 401, 453
 Böttcher, M. & Dermer, C. D. 1999, *Astropart. Phys.*, 11, 113
 Böttcher, M. & Fryer, C. L. 2001, *ApJ*, 547, 338
 Chevalier, R. A. 1977, in *Supernovae*, ed. D. N. Schramm, (Dordrecht: Reidel) 53
 Chevalier, R. A. & Fransson, C. 1992, *ApJ*, 395, 540
 Cook, G. B., Shapiro, S. L. & Teukolsky, S. A. 1994, *ApJ*, 424, 823
 Davidson, K. & Fesen, R. A. 1985, *ARA&A*, 23, 119
 Dermer, C. D. 1995, *ApJ*, 446, L63
 Galama, T. J. et al. 2000, *ApJ*, 536, 185
 Frail, D. A., Waxman, E. & Kulkarni, S. R. 2000, *ApJ*, 537, 191
 Frail, D. A. et al. 2000, *ApJ*, 538, L129
 Frail, D. A. et al. 2001, *astro-ph/0102282*
 Fryer, C. & Woosley, S. 2001, *Nature*, 411, 31
 Harrison, F. A. et al. 2001, *ApJ*, 559, 123
 Hester, J. J. et al. 1996, *ApJ*, 456, 225
 Hurley, K. et al. 1994, *Nature*, 372, 652
 Inoue, S. & Takahara, F. 1996, *ApJ*, 463, 555
 Inoue, S. & Takahara, F. 1997, *Prog. Theo. Phys.*, 98, 807
 In 't Zand, J. J. M. et al. 2001, 559, 710
 Lazzati, D. et al. 2001a, *ApJ*, 556, 471
 Lazzati, D. et al. 2001b, *A&A*, 996, 1002
 Lazzati, D., Campana, S. & Ghisellini, G. 1999, *MNRAS*, 304, L11
 Lindblom, L., Tohline, J. E. & Vallisneri, M. 2001, *Phys. Rev. Lett.*, 86, 1152
 Masetti, N. et al. 2001, *A&A*, 374, 382
 Mészáros, P. 2001, *Sci*, 291, 79
 Mészáros, P. & Rees, M. J. 1997, *ApJ*, 476, 232
 Pacini, F. 1967, *Nature*, 216, 567
 Pacini, F. & Salvati, M. 1973, *ApJ* 186, 249 (PS73)
 Paerels, F., Kuulkers, E., Heise, J. & Liedahl, D. A. 2000, *ApJ*, 535, L25
 Panaitescu, A. & Kumar, P. 2000, *ApJ*, 543, 66
 Panaitescu, A. & Kumar, P. 2001a, *ApJ*, 554, 667
 Panaitescu, A. & Kumar, P. 2001b, *ApJ*, 560, L49
 Piran, T. 1999, *PhysRep*, 314, 575
 Piro, L. et al. 1999, *ApJ*, 514, L73
 Piro, L. et al. 2000, *Sci*, 290, 955
 Piro, L. et al. 2001, *ApJ*, 558, 442
 Porciani, C. & Madau, P. 2001, *ApJ*, 548, 522
 Rees, M. J. & Mészáros, P. 2000, *ApJ*, 545, L73
 Reynolds, S. P. & Chevalier, R. A. 1984, *ApJ*, 278, 630
 Salgado, M., Bonazzola, S., Gourgoulhon, E. & Haensel, P. 1994, *A&A*, 291, 155
 Sankrit, R. & Hester, J. J. 1997, *ApJ*, 491, 796
 Sari, R. & Esin, A. A. 2001, *ApJ*, 548, 787 (SE01)
 Sari, R., Piran, T. & Narayan, R. 1998, *ApJ*, 497, L17
 Sikora, M. in 4th Compton Symposium, eds. C. D. Dermer, M. S. Strickman & J. D. Kurfess, AIP Conf. Proc. 410, p494
 Sikora, M., Sol, H., Begelman, M. C. & Madejski, G. M. 1996, *MNRAS*, 280, 781
 Stecker, F. W. & de Jager, O. C. 1998, *A&A*, 334, L85
 Totani, T. 2000, *ApJ*, 536, L23

van Paradijs J., Kouveliotou C., Wijers R.A.M.J., 2000, ARA&A, 38, 379
 Vietri, M. et al. 2001, ApJ, 550, L43
 Vietri, M. & Stella, L. 1998, ApJ, 507, L45 (VS98)
 Voges, W. et al. 1999, A&A, 349, 389
 Weth, C., Mészáros, P., Kallman, T. & Rees, M. J. 2000, ApJ, 534, 581

Wijers, R. A. M. J. & Galama, T. J. 1999, ApJ, 523, 177
 Yonetoku, D. et al. 2000, PASJ, 52, 509
 Yonetoku, D. et al. 2001, ApJ, 557, L23
 Yoshida, A. et al. 2001, ApJ, 557, L27
 Zhang, B. & Mészáros P. 2001, ApJ, 559, 110 (ZM01)

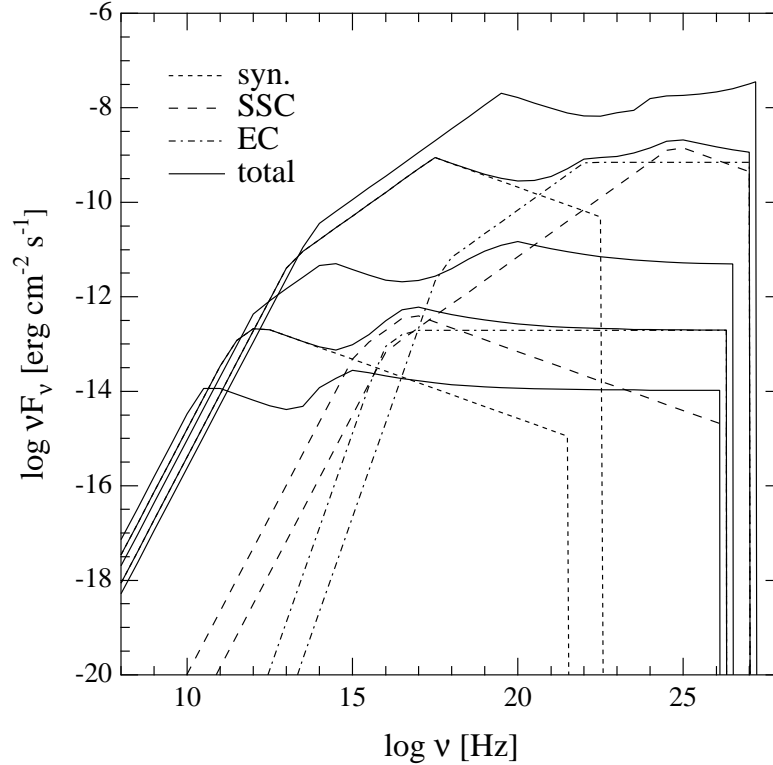


FIG. 1.— The time-dependent afterglow spectra for our fiducial parameters at $t=1$ second, 1 minute, 1 hour, 1 day and 15 days after the GRB, from top to bottom. The curves for $t=1$ minute and $t=1$ day show the decomposition into synchrotron (dotted), SSC (dashed) and EC (dot-dashed) components.

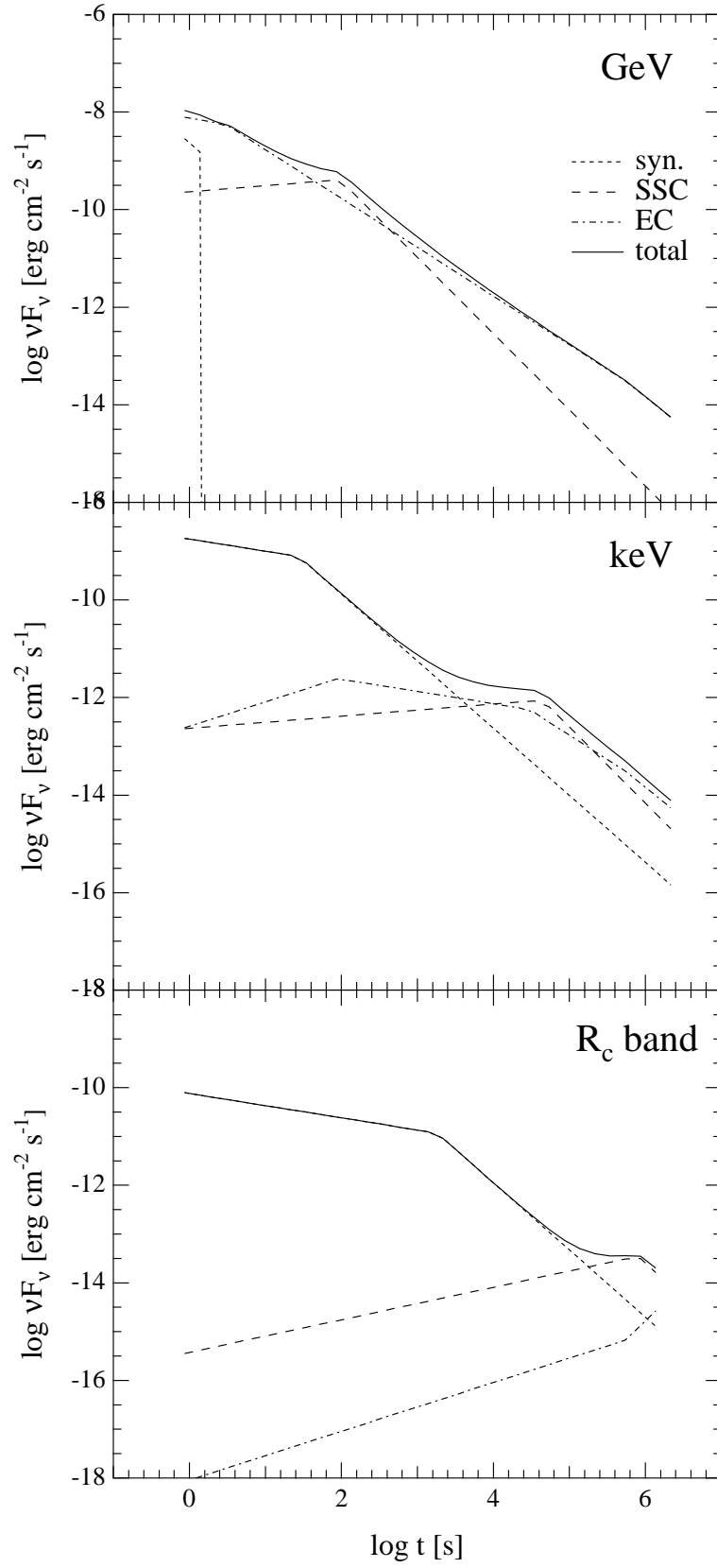


FIG. 2.— The afterglow light curves for our fiducial parameters at $\nu = 2.4 \times 10^{23}$ Hz (1 GeV, top), $\nu = 2.4 \times 10^{17}$ Hz (1 keV, middle) and $\nu = 4.5 \times 10^{14}$ Hz (R_c band, bottom). The synchrotron (short-dashed), SSC (long-dashed) and EC (dot-dashed) components are also shown separately.